ACCEPT/REJECT CRITERIA FOR STRUCTURAL CERAMICS:

PART 2: SOME EFFECTS OF CAVITIES ON THE FRACTURE OF CERAMICS
II. SPHERICAL CAVITIES

A.G. Evans
Rockwell International Science Center
Thousand Oaks, California 91360

D.R. Biswas and R.M. Fulrath
Materials and Molecular Research Division
Lawrence Berkeley Laboratory and Department of Materials Science
and Mineral Engineering, University of California
Berkeley, California 94720

ABSTRACT

Fracture probabilities associated with spherical cavities have been analyzed, by combining principles of fracture mechanics and fracture statistics. The analysis considers that fracture occurs from a distribution of cracks located at the cavity surfaces. It predicts effects of cavity size and cavity volume content (porosity) on strength, that depend sensitively on the flaw population vis-a-vis the cavity size distribution. The theory is shown to have limit solutions that coincide with several earlier models of fracture, derived for porous ceramics. The predicted effects of pore size on strength are compared with some available data.

INTRODUCTION

In a companion paper,[1] a general approach for predicting fracture from cavities, by combining linear elastic fracture mechanics solutions with statistics solutions, has been described: and applied to cylindrical cavities. The method is extended in this paper to include the analogous considerations pertinent to spherical cavities. Again, the emphasis is on the approach, recognizing that the available fracture mechanics and statistics solutions are inadequate in some instances. Improved solutions can be incorporated, using the same general approach, as they emerge.

Fracture mechanics solutions for cracks emanating from the surface of spherical cavities are examined in the first part of the paper. The best available solutions are then combined with statistical results - derived for the stress field around spherical voids - to obtain preliminary relations between the fracture probability, the cavity size and the surface flaw size distribution. Finally, the implications of the analysis for the effect on strength of individual voids and void arrays (porosity) are discussed.

STRESS INTENSITY FACTOR SOLUTIONS

The first problem of interest pertains to the equatorial annular crack emanating from a spherical cavity (Fig. 1). The tensile stress σ_z normal to the crack plane, for a remote stress σ_∞ is[2]

$$\sigma_z = \sigma_\infty \left[1 + \frac{(4-5\nu)}{2(7-5\nu)}\left(\frac{r}{x}\right)^3 + \frac{9}{2(7-5\nu)}\left(\frac{r}{x}\right)^5\right], (x \geq r) \quad (1)$$

$$\sigma_z = 0, \quad (x < r)$$

where ν is Poisson's ratio and x is the distance from the center of the sphere (Fig. 1). An estimate of the stress intensity factor for the annular crack can be obtained[1] by imposing this stress onto the surface of a penny crack (Fig. 1).

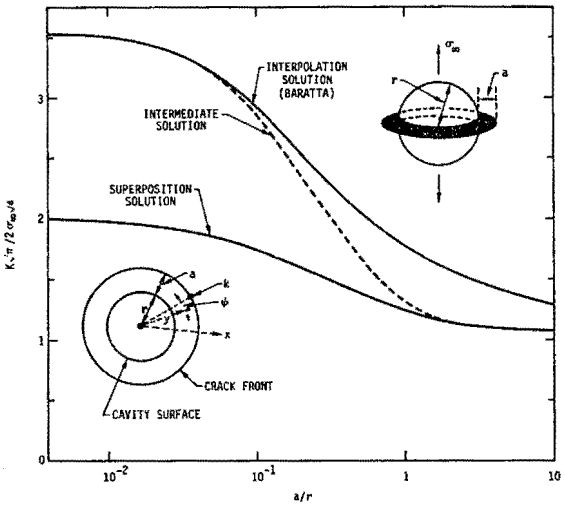

Fig. 1. Stress intensity factor solutions for an annular crack emanating from a spherical cavity.

The general linear superposition function used for three-dimensional problems of this type is,[1,3]

$$K_I\Big/_{\psi=0} = \frac{2}{(\pi a)^{3/2}} \int_0^{\pi} \int_0^{a} \frac{\sigma(y,\psi)\, y\left[1-(y/a)^2\right]^{1/2}}{\left[1-2(y/a)\cos\psi+(y/a)^2\right]} \, dy\, d\psi \quad (2)$$

where y is the radial distance from the crack center, ψ is the angular location with respect to the crack front position of interest and a is the crack radius (see Figs. 1,2). The symmetry of the annular crack problem provides the following simplification; ψ=0 and x=y. Substituting Eqn. (1) into (2) then gives;

$$\frac{\sqrt{\pi}\,K_I}{2\sigma_\infty\sqrt{a}} = \int_{(r/a)}^{1} \frac{[2(7-5\nu) + (4-5\nu)(r/a)^3\chi^{-3} + 9(r/a)^5\chi^{-5}]}{2(7-5\nu)(1-\chi^2)^{1/2}}\,\chi\,d\chi \qquad (3)$$

where $\chi=y/a$. Integration of Eqn. (3) for $\nu=0.2$ gives the result plotted in Fig. 1. Studies on radial cracks emanating from cylindrical cavities[1,3] have indicated that this type of solution is most pertinent for relatively large cracks ($a/r \gg 1$). For smaller cracks, the presence of the cavity surface allows an enhanced crack opening that tends to augment K_I (toward the edge crack solution, $\sqrt{\pi}K/2\sigma_\infty\sqrt{a}=3.52$). This small crack limit was recognized by Baratta[4] in his development of an interpolation solution for the annular crack problem. The interpolation solution for $\nu=0.2$ is plotted in Fig. 1. This solution predicts K values appreciably larger than the superposition solution, for all a/r. Additional studies are clearly needed; but for present purposes, it is assumed that the superposition solution is the more precise at large a/r ($\gg 1$) and that the interpolation solution is superior at small a/r ($< 10^{-1}$) - suggesting the intermediate solution plotted in Fig. 1.

The second configuration of interest is the partial circular crack on the surface of a spherical cavity (Fig. 2). For this case, consider the crack shown in Fig. 2, located such that the crack plane is normal to the applied tension. Superposition solutions for surface cracks usually invoke a symmetric image crack (and then apply a surface correction). However, in the present problem, the curvature of the surface perturbs the symmetry (Fig. 2). An approximate solution is thus obtained by assuming that the stress field for the crack/image combination is symmetric about the surface tangent 00' (Fig. 2). This solution should be most pertinent at small a/r, where the surface perturbation is small.

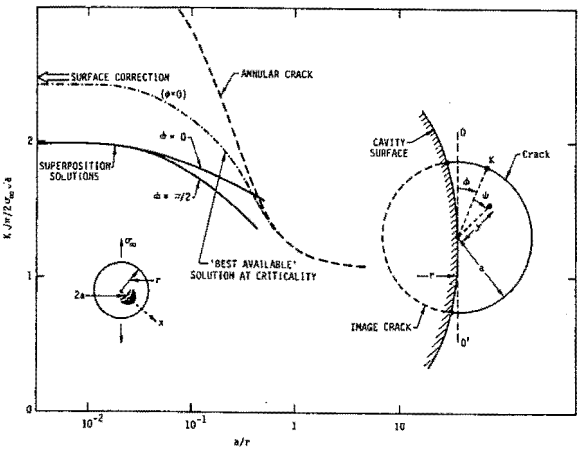

Fig. 2. Stress intensity factor solutions for an annular crack emanating from a spherical cavity.

The solution is obtained by noting that x and y are related by;

$$x = r + y\sin(\phi+\psi), \qquad (4)$$

where ϕ is the angle shown in Fig. 2; then, substituting Eqn. (1) into Eqn. (2) gives;

$$\frac{\sqrt{\pi}\,K_I}{2\sigma_\infty\sqrt{a}} = \int_0^1\int_0^\pi \chi(1-\chi^2)^{1/2} \frac{[2(7-5\nu)+(4-5\nu)(1+\chi\gamma\sin(\psi+\phi))^{-3}+9(1+\chi\gamma\sin(\psi+\phi))^{-5}]}{2[1-2\chi\cos\psi+\chi^2](7-5\nu)}\,d\chi\,d\psi \qquad (5)$$

where $\gamma = r/a$. Integration of Eqn. (5) for $\phi = 0$ and $\pi/2$ yields the results plotted in Fig. 2, for $\nu = 0.2$. The stress intensity factor at $\phi = \pi/2$ is likely to be slightly enhanced by the presence of the surface,[1] by up to ~ 1.05 for small a/r; while K at $\phi = 0$ may be augmented by up to ~ 1.23. Allowing for possible corrections of this magnitude, a comparison of the partial circular crack results with the annular crack result indicates that K for the former is clearly the smaller at small a/r (< 0.5). Partial circular cracks in this size range should thus extend unstably in the presence of a critical applied stress. However, for larger a/r ($\gg 1$) the stress intensity factor for the annular crack may be smaller; suggesting the possible subcritical extension of a partial circular crack into an annular crack (analogous to the behavior proposed for cylindrical cavities)[1]. These considerations suggest that the resultant stress intensity factor at criticality might exhibit the form depicted in Fig. 2; which is used herein as the "best available" solution for surface cracks associated with spherical cavities. A convenient analytic expression for K deduced from Fig. 2 is;

$$\sqrt{\pi}\,K/2\,\sigma_\infty\sqrt{a} = 1 + 0.3[0.21 + a/r]^{-1} \qquad (6)$$

STATISTICAL ANALYSIS

Fracture probabilities for spherical cavities at small a/r have been evaluated[5] assuming a normal tensile stress criterion, and using Weibull's multiaxial stress method for flaws of a single population distributed throughout the volume of the body. A different analysis is presented in this paper, which uses a more fundamental statistical method for treating multiaxial states of stress[6,7], and applies the approach to a distribution of flaws at the cavity surface. For flaws located at the surface of a spherical cavity, the only stresses that exist are the tangential stresses,[8]

$$\sigma_\theta = \frac{3\sigma_\infty}{2(7-5\nu)}[4-5\nu+5\cos 2\theta]$$

$$\sigma_\alpha = \frac{3\sigma_\infty}{2(7-5\nu)}[5\nu\cos 2\theta - 1] \qquad (7)$$

where θ is the angular coordinate with respect to the equatorial plane (Fig. 3).

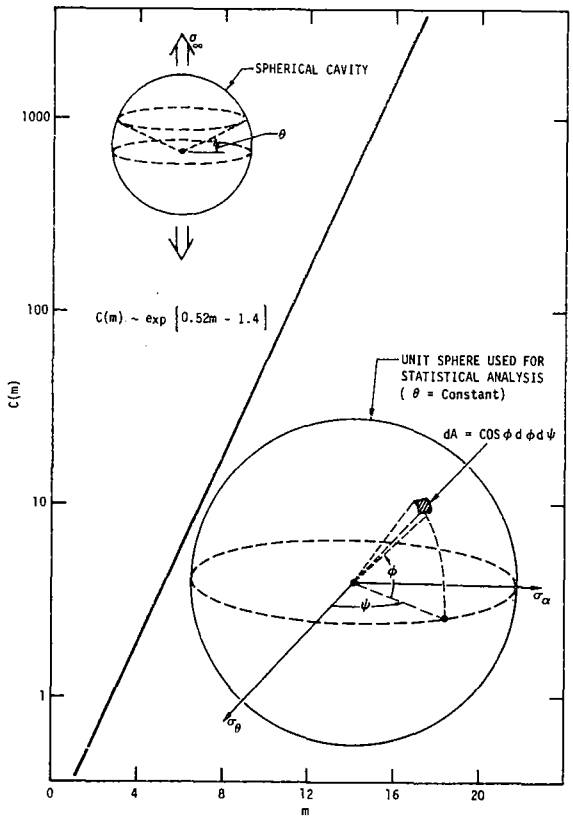

Fig. 3. The statistical parameter C(m) derived for a spherical cavity subjected to a uniaxial tension σ_∞. Also shown is the angular coordinate θ used to describe the stress variation, and the unit sphere used for statistical analysis.

The statistical problem is thus concerned with the analysis of biaxial fracture. Only the zone of tension is of interest.[1] For $\nu = 0.2$, σ_θ is tensile in the range $0.35\pi < \theta < -0.35$. The corresponding σ_α is compressive. The tension/compression quadrant thus pertains. The fracture criterion that has most successfully described multiaxial fracture[7] (as well as angular dependencies of fracture[9]) in ceramics is that based on the co-planar strain energy release rate#:

$$S_T^2 = \sigma_n^2 + \frac{4\tau_m^2}{(2-\nu)^2} \qquad (8)$$

where S_T is the flaw extension stress in equi-triaxial tension, σ_n is the tensile stress normal to the flaw and τ_m is the maximum in-plane shear stress. For flaws located in the surface element dA of a unit sphere (Fig. 3) that contains a complete sampling of flaws of all (random) orientations,[7] the stresses σ_n and σ_m are related to the stresses σ_θ and σ_α and the angles φ and ψ defined in Fig. 3 by;

$$\sigma_n^2 = \cos^4\phi[\sigma_\alpha^2\sin^4\psi + \sigma_\theta^2\cos^4\psi + 2\sigma_\alpha\sigma_\theta\cos^2\psi\sin^2\psi]$$

$$\tau_m^2 = \cos^2\phi[\sigma_\alpha^2\sin^2\psi(1-\cos^2\phi\sin^2\psi) \qquad (9)$$

$$+\sigma_\theta^2\cos^2\psi(1-\cos^2\phi\cos^2\psi) + 2\sigma_\theta\sigma_\alpha\cos^2\phi\cos^2\psi\sin^2\psi]$$

If the strength distribution in triaxial tension is now defined[7] by a Weibull-type function, with a scale parameter S_o^* and a shape parameter k,

$$g(S_T) = \left(\frac{S_T}{S_o^*}\right)^k, \qquad (10)$$

consideration of the eight equivalent areal elements, $dA = \cos\phi d\phi d\psi$ (Fig. 3), allows the biaxial strength distribution function to be derived, for given θ[7];

$$g(S_B)\Big|_\theta = \left(\frac{2}{\pi}\right)\int_0^{\psi^*(\theta)}\int_0^{\pi/2}\left(\frac{S_T}{S_o^*}\right)^k \cos\phi d\phi d\psi dS_T \qquad (11)$$

where $\psi^*(\theta)$ is the value of ψ at which σ_n first becomes negative, as deduced from Eqn. (9). Then substituting Eqn. (11) into the weakest link formulation,[1,6,7]

$$\Phi(S) = 1 - \exp\left[-\int_A dA \int_0^S g(S)dS\right] \qquad (12)$$

allows the probability of fracture from the cavity to be expressed as;

#This criterion has been used with good success for stress conditions wherein σ_n is tensile. It cannot be expected to apply when σ_n is compressive. In the present analysis, the fracture probability when σ_n is compressive is assumed to be zero. This will lead to underestimates of the failure probability, by an amount that depends on the initial opening of the flaw,[10] i.e., if the initial crack opening is small, as expected for the flaws of present interest, the underestimate will also be small.

$$-\ln[1-\Phi(S_\infty^c)] =$$

$$8r^2 \int_0^{S_\infty} \left(\frac{S_\infty}{S_o^*}\right)^k dS_\infty \int_0^{0.35\pi} \int_0^{\psi^*(\theta)} \int_0^{\pi/2} \cos\phi\cos\theta$$

$$\left\{\frac{9\cos^2\phi}{4(7-5\nu)^2}\right. \left[\cos^2\phi\,(4-5\nu+5\cos2\theta)^2\cos^4\psi\right.$$

$$+ (5\nu\cos2\theta-1)^2\cos^2\phi\sin^4\psi$$

$$+ 2(4-5\nu+5\cos2\theta)(5\nu\cos2\theta-1)\cos^2\phi\cos^2\psi\sin^2\psi$$

$$+ (4/(2-\nu)^2)\,(5\nu\cos2\theta-1)^2\sin^2\psi(1-\cos^2\phi\sin^2\psi)$$

$$+ (4-5\nu+5\cos2\theta)^2\cos^2\psi(1-\cos^2\phi\cos^2\psi) + 2(4-5\nu$$

$$+ 5\cos2\theta)$$

$$\left.\left.(5\nu\cos2\theta-1)\cos^2\phi\cos^2\psi\sin^2\psi\right]\right\}^{(k+1)/2} d\psi d\phi d\theta \quad (13)$$

$$\equiv 8r^2 B(k,\nu)\; S_o^*(S_\infty^c/S_o^*)^{k+1}/(k+1)$$

where S_∞^c is the value of the applied stress σ_∞ at fracture, in the presence of the cavity. The equivalent fracture probability for uniaxial tension has been derived as;[7]

$$-\ln[1-\Phi(S_\infty^u)] = A_g I_u(k,\nu)\; S_o^*\,(S_\infty^u/S_o^*)^{k+1}/(k+1) \quad (14)$$

where A_g is the gauge surface area, S_∞^u is the applied stress at fracture and $I_u(k,\nu)$ is a function that relates the uniaxial strength to the triaxial strength.[7] Expressing Eqn. (14) in a notation consistent with the more conventional Weibull formulism,[11]

$$-\ln[1-\Phi(S_\infty^u)] = A_g(S_\infty^u/S_o)^m\,, \quad (15)$$

where the scale and shape functions are now S_o and m, and substituting into Eqn. (13), the fracture probability for the cavity becomes;

$$-\ln[1-\Phi(S_\infty^c)] = 8r^2\; C(m,\nu)(S_\infty^c/S_o)^m \quad (16)$$

where C(m) is plotted in Fig. 3, for $\nu = 0.2$. A useful analytic approximation is, $C(m) \sim \exp[0.52m-1.4]$. Comparison with the companion paper[1] indicates that, for the same area of cavity surface and the same flaw population, the probability of fracture from a spherical cavity is smaller than that from a cylindrical cavity.

Now, useing the same procedure described for the cylindrical cavity,[1] a stress gradient correction can be applied. The effective flaw strength S^* derived from Eqn. (6) is;

$$\frac{S}{S^*} = 0.33 + 2(0.11 - 0.21\alpha)^{1/2}\cosh(\lambda/3) \equiv D(\alpha)$$

where

$$\lambda = \cosh^{-1}\,(0.037 + 0.021\alpha)/(0.11 - 0.21\alpha)^{3/2} \quad (17)$$

and

$$\alpha = (1/r)(K_c/S^*)^2$$

This solution applies for $\alpha<0.52$; the corresponding sinh solution applies of $\alpha>0.52$. The function $D(\alpha)$ is plotted in Fig. 4.

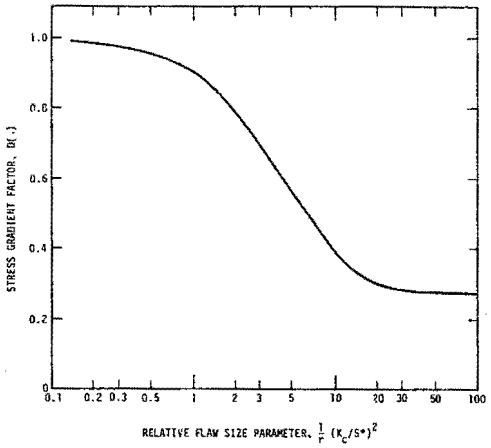

Fig. 4. The stress gradient factor $D(\alpha)$ for a spherical cavity.

Assuming that a similar relation pertains for all flaw locations and orientations in the tensile range,[1] the fracture probability becomes;

$$-\ln[1-\Phi(\hat{S}_\infty)] = 8r^2\left(\frac{\hat{S}_\infty}{S_o}\right)^m C(m)\; D^m(\alpha) \quad (18)$$

where $\hat{S}_\infty$ is the new value of the applied stress at fracture. The fracture probabilities predicted by Eqn. (18) are plotted in Fig. 5, as a function of the normalized strength $(\hat{S}_\infty/S_o)$, for several relative void radii (r/r_o) and a typical m of 4; r_o and $K_c^2/r_o S_o^2$ are chosen to be unity. The probabilities obtained from Eqn. (16) are also plotted for comparison. The same trends found for the cylindrical cavity are evident, but are accompanied by smaller reductions in the fracture probability.

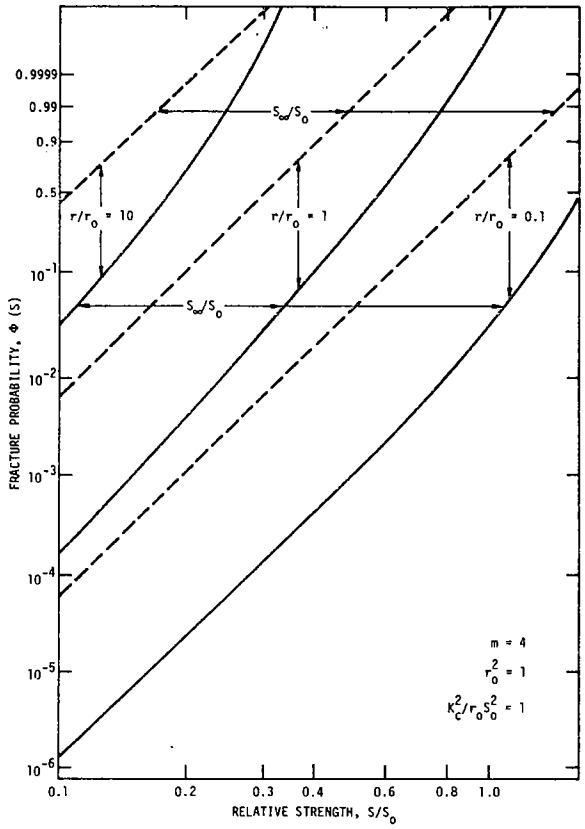

Fig. 5. Fracture probabilities for spherical cavities plotted as a function of the relative strength, for a value of the shape parameter m = 4.

EFFECTS OF POROSITY ON STRENGTH

Cavity Arrays

In porous ceramics, if the porosity is low enough that pore interaction effects cannot occur, the probability of fracture from flaws distributed at the pore surfaces can be determined, in the usual way[5,6,7] from the product of the survival probabilities of individual cavities. For a pore size distribution $\phi(r)dr$ (i.e., the fraction of pores in the size range r to r+dr) the probability of failure $\Phi_T(\hat{S}_\infty)$ from a volume V subjected to uniform tension, derived from Eqn. (18), is;

$$-\ell n[1-\Phi_T(\hat{S}_\infty)] = 4NV\left(\frac{\hat{S}_\infty}{S_o}\right)^m C(m)\int_{r_{min}}^{r_{max}} \phi(r) r^2 D^m(\alpha)\,dr \qquad (19)$$

where r_{max} and r_{min} are the radii of the largest and smallest pores, respectively; N is the number of pores in unit volume, which is related to the porosity, P, by;

$$P = \frac{4\pi}{3}\langle r^3\rangle N \qquad (20)$$

For pores of uniform size $\bar{r}$, Eqn. (19) becomes;

$$-\ell n[1-\Phi_T(\hat{S}_\infty)] = \frac{3PV}{\pi \bar{r}}\left(\frac{\hat{S}_\infty}{S_o}\right)^m C(m)D^m(\alpha) \qquad (21)$$

Hence, in the limit $a/r \to 0$, where D is independent of r, the fracture probability for a fixed flaw population is expected to slightly increase, (i.e., the strength to decrease) as the pore radius decreases. This condition arises because the relative cavity surface area increases as the cavity radius decreases, permitting a more extensive sampling of the flaw population. (It should be noted that this cavity size dependence does not exist when fracture initiates from volume distributed flaws[5]). However, the trend with cavity radius is counteracted by the decrease in D, associated with the concurrent increase in a/r. The resultant variation of strength with the relative cavity radius (r/r_o) at constant porosity (0.1) is plotted at constant probability in Fig. 6. These strengths scale with porosity through the sample proportionality, p-1/m. (It is re-emphasized that the analysis is only valid when there is no significant pore interaction; the implications must, therefore, be restricted to low porosities.)

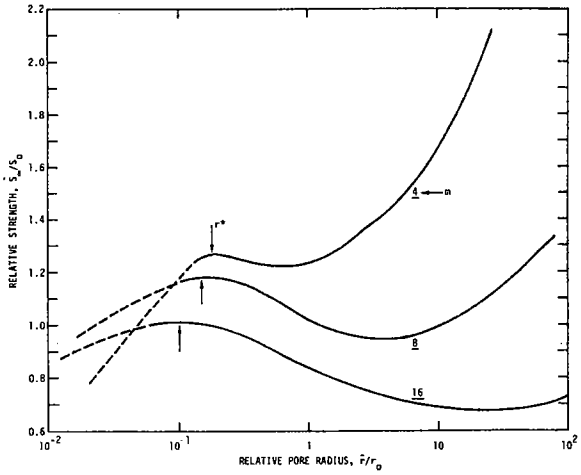

Fig. 6. Effects of relative pore radius $\bar{r}$ on the relative fracture strength at constant probability, plotted for three m values and a porosity of 0.1.

It is evident from the quite extensive regime of increasing strength (with decreasing void radius) that the influence of the stress gradient parameter D is dominant over a wide range of void radii. The inference of this result is that the strength for a fixed flaw population can be maximized either by collecting all of the porosity in a small number of large voids, or by producing voids of optimum size, r*. However, the former will not normally be a practicable solution. The latter should be feasible, but the possibility of other modes of fracture occurring at small void sizes may pre-empt the development of a strength maximum in many ceramic polycrystals. Also, for various microstructural reasons, the flaw population may change as the pore size changes, (e.g., an increase in the scale factor S_o as the pore size increases), leading to more substantial effects of pore size on strength than predicted by Fig. 6.

There are very few data in the literature concerning the effects of pore size on strength. The most comprehensive are data on borosilicate glass obtained by Bertolotti and Fulrath.[12] These data re-examined in the context of the present model, even though the uncertain influence of surface cracks (machining flaws) on the fracture data detracts from the utility of the correlation. For comparison with the model, the appropriate values of $D(\alpha)$ are first obtained for each void size, using a K_C of 0.7 MPa $\sqrt{m}$.[13] Then, the shape parameter m is estimated from the pore volume dependence of the strength at low porosity ($S \propto P^{-1/m}$) - and found to be in the range 10 to 20. The fracture strength, relative to the strength of the samples with the largest voids, can then be computed at constant failure probability, by direct insertion of these quantities into Eqn. (21). The results for m values of 10 to 20 are plotted in Fig. 7; also plotted on the figure are the data obtained from Bertolotti and Fulrath, at three levels of porosity. The predictions tend to slightly underestimate the measured pore size dependence. The uncertainty in the origin of failure for the test samples prevents definitive conclusions from the comparison. More precise experiments are needed to determine the principal deficiencies of the theory, in its present form.

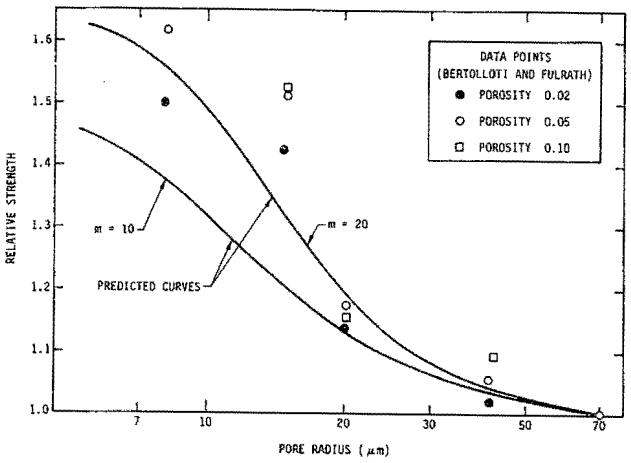

Fig. 7. A comparison of the predicted effects of pore radius on the strength (at constant porosity and constant probability) with data obtained for borosilicate glass.

Isolated Cavities

The effects of the size of an isolated cavity on strength can be deduced directly from Eqn. (18). These effects are plotted at constant probability in Fig. 8, to demonstrate that there are no simple relations between defect size and strength. However, a close examination of Eqn. (18) indicates important fracture trends, and illustrates the relation between the present analysis and earlier models of fracture from voids.[14,15] For large values of the shape parameter m, there is a high probability of a flaw at the large extreme of the population being located at the position of maximum tension on the cavity surface. Therefore, if α is small (small a/r), $D(\alpha) \to 1$, and Eqn. (16) applies. The strength will then be related to that of a sample without cavities (Eqn. 15) by the factor $C(m)^{-1/m}$. Applying the analytic approximation for C(m) indicated on Fig. 3, this factor (at large m) is ~1.92, i.e., equal to the stress concentration factor. The connection with the stress concentration factor model is thus established. Alternately if α is large, $D(\alpha)$ tends to 0.5 and exactly cancels C(m) in Eqn. (18). The strength is thus identical to that expected for a crack located at the cavity, i.e., it is equal to the strength in tension given by Eqn. (15). The connection with the cavity/crack equivalence model is thus apparent. For small values of m, there is a low probability of an extreme value flaw being located at the position of maximum tension.

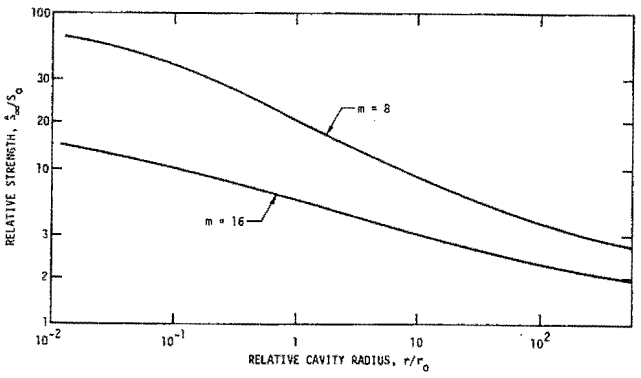

Fig. 8. Predicted effect of the relative cavity radius on the relative strength for a body containing a single cavity of the specified size. Results are presented for two values of the shape parameter m.

Hence, C(m) ~ 1 (see Fig. 3), and the influence of the cavity on strength is quite minimal. For small α, the effect of the cavity tends to reduce to a level similar to that expected from the increased surface area provided by the cavity. For larger α the effect is even smaller. The connection with models based on the void area is thus established. For intermediate values of m and the present model predicts strength effects that range continually between the limit solutions provided by the earlier models. It should thus exhibit the versatility needed to account for many of the trends observed experimentally. However, it is emphasized that certain important phenomena are not yet incorporated in the model (such as the linking of subsurface pores with surface cracks), and that the stress intensity factor solutions are approximate. Therefore, much additional analysis is still needed to develop the present model into a universal model of cavity fracture.

Finally, the prediction of failure from isolated cavities in dense ceramics can directly utilize Eqn. (18), when the cavities are nearly spherical in shape. The probability of service failure from cavities Φ_F, at a stress level σ_A, based on a nondestructive characterization of the cavity dimensions, if all cavities with an interpreted cavity radius r_i^o are accepted, is;[16]

$$\Phi_F(\sigma_A, r_i^o) = \int_0^{\sigma_A} \int_0^{r_i^o} \int_0^{\infty} \phi(\hat{S}_\infty)\phi(r_i/r)\phi(r)dr\,dr_i\,dS_\infty \qquad (22)$$

where $\phi(\hat{S}_\infty)dS$ is the derivative of Eqn. (18); $\phi(r_i/r)dr_i$ is the probability that the nondestructively interpreted cavity radius r_i is in the range r_i to r_i+dr_i, given that its actual radius is r; $\phi(r)dr$ is the cavity radius distribution in the material. The concepts developed in this paper are thus an important constituent in any nondestructive failure prediction scheme for structural ceramics. The details are described in a separate publication.[16]

CONCLUDING REMARKS

Fracture from spherical cavities has been analyzed by considering that fracture occurs by the extension of a population of cracks located at the cavity surface. The analysis indicates trends in the fracture condition with cavity size and volume, that depend on the flaw size distribution relative to the cavity size. It has been shown that the present analysis provides limit solutions that are analagous to several earlier models of cavity fracture; thereby, providing the required connective link between the models. The analysis is only regarded as preliminary because the presently available stress intensity factor solutions are inadequate and because several important subcritical flaw linking phenomena have not yet been included in the analysis. Much additional study is needed to evolve a model of the above type that has universal utility for cavity fracture.

The analysis has been used to predict effects of pore volume (porosity) on strength that should be pertinent to small pore volumes (i.e., no pore interaction effects). The predictions have been compared with some available data for borosilicate glass. Although the correspondence was quite good, little value was gained from the correlation, because of the uncertain origins of fracture in the fracture tests. Precise studies are needed to correlate with the theory. The appropriate tests have recently been initiated.

ACKNOWLEDGMENT

This research was sponsored by the Center for Advanced NDE, operated by the Science Center, Rockwell International, for the Defense Advanced Research Projects and the Air Force Materials Laboratory under Contract F33615-74-C-5180.

REFERENCES

1. A.G. Evans, D.R. Biswas and R.M. Fulrath, submitted to Jnl. Amer. Ceram. Soc.
2. S. Timoshenko and J.N. Goodier, Theory of Elasticity (McGraw-Hill, N.Y.) 1951.
3. R.C. Shah, ASTM STP 590 (1976) 429.
4. F. Baratta, Jnl. Amer. Ceram. Soc., in press.
5. O. Vardar, I. Finnie, D.R. Biswas and R.M. Fulrath, Int. J. Frac. 13 (1977) 215.
6. S. Batdorf and J.G. Crose, Jnl. Appl. Mech. 41 (1974).
7. A.G. Evans, Jnl. Amer. Ceram. Soc., 61 May/June 1978.
8. J.N. Goodier, Trans ASME (Jnl. Apl. Mechs.) 55 (1933) 39.
9. J.J. Petrovic and M.G. Mendiratta, Jnl. Amer. Ceram. Soc. 60 (1977) 463.
10. M. Adams and G. Sines, Jnl. Amer. Ceram. Soc. 59 (1976) 300.
11. W. Weibull, Jnl. Appl. Mech. 18 (1951) 193.
12. R. Bertolotti and R.M. Fulrath, Jnl. Amer. Ceram. Soc., 50 (1967) 561.
13. S.M. Wiederhorn, Jnl. Amer. Ceram. Soc. 52 (1969) 99.
14. S.C. Carniglia, Jnl. Amer. Ceram. Soc. 56 (1973) 547.
15. R.W. Rice, Treatise on Materials Science and Technology 11 (1977) 199.
16. J.M. Richardson and A.G. Evans, to be published.